

# Refining centromedian nucleus stimulation for generalized epilepsy with targeting and mechanistic insights from intraoperative electrophysiology

Received: 25 March 2024

Accepted: 16 May 2025

Published online: 06 June 2025

 Check for updates

Jonathan C. Ho <sup>1,2,5</sup>, Thandar Aung<sup>1,3,5</sup>, Arianna Damiani <sup>2,4</sup>, Lilly Tang<sup>1,2</sup>, Arka N. Mallela <sup>4</sup>, Donald J. Crammond<sup>1,4</sup> & Jorge A. González-Martínez<sup>1,4</sup> 

Epilepsy affects 65 million people worldwide, with 30% suffering from drug-resistant epilepsy. While surgical resection is the primary treatment, its application is limited in generalized epilepsy. Centromedian nucleus neurostimulation offers a promising alternative, yet its mechanisms remain unclear, limiting target optimization. We present a multimodal approach integrating intraoperative thalamic and sub-scalp electroencephalogram recordings with post-implant reconstructions to define neural targets affected by centromedian nucleus stimulation. We find that stimulating low-activity regions near the centromedian nucleus, particularly the white matter of internal medullary lamina, induces significant cortical delta power increases greater than stimulation within high-activity areas inside the nucleus. Implantation in these low-activity targets results in greater than 50% seizure reduction in all three subjects. These findings suggest that seizure control primarily involves stimulating white matter regions such as the internal medullary lamina rather than the centromedian nucleus itself. A personalized, electrophysiology-guided implantation approach may enhance neurostimulation efficacy in drug-resistant epilepsy.

Epilepsy is the fourth most common chronic neurological disorder worldwide, affecting ~65 million people<sup>1</sup>. Among this group, thirty percent suffer from drug-resistant epilepsy (DRE), which requires the failure of at least two appropriate antiepileptic medications<sup>2,3</sup>. These patients suffer from significant impairments in their quality of life, education, and employment<sup>2,3</sup>. Surgical resection of the epileptogenic zone is often the primary therapeutic option for seizure control. However, many patients are ineligible for this intervention due to the involvement of eloquent cortical regions, widespread bilateral seizure foci, or a diagnosis of generalized epilepsy<sup>4</sup>. These limitations result in a considerable subset of patients with limited therapeutic options who

experience inadequate seizure control, further deterioration in their quality of life, and substantial emotional and economic burdens<sup>4,5</sup>. Neuromodulation, such as thalamic closed-loop responsive neurostimulation (RNS) and open-loop deep brain stimulation (DBS) of the thalamus, has emerged as a viable alternative for these patients<sup>6</sup>. Although both the anterior nucleus (ANT) and centromedian nucleus (CM) neuromodulation have demonstrated potential in reducing seizure frequency, significant challenges remain in optimizing these therapies to maximize therapeutic outcomes<sup>7–9</sup>.

While ANT-DBS has shown considerable efficacy in treating drug-resistant temporal lobe epilepsy<sup>9</sup>, there is accumulating evidence

<sup>1</sup>School of Medicine, University of Pittsburgh, Pittsburgh, PA, USA. <sup>2</sup>Rehab and Neural Engineering Labs, University of Pittsburgh, Pittsburgh, PA, USA.

<sup>3</sup>Department of Neurology, University of Pittsburgh, Pittsburgh, PA, USA. <sup>4</sup>Department of Neurological Surgery, University of Pittsburgh, Pittsburgh, PA, USA.

<sup>5</sup>These authors contributed equally: Jonathan C. Ho, Thandar Aung. ✉ e-mail: [gonzalezjo@upmc.edu](mailto:gonzalezjo@upmc.edu)

suggesting that CM stimulation could play a critical role in managing generalized epilepsy and associated syndromes such as Lennox-Gastaut Syndrome<sup>6,8,10–16</sup>. The CM, the largest nucleus within the intralaminar thalamic group, is intricately connected with the brainstem reticular formation and sensorimotor cortices, with the latter being implicated in the generation of synchronous spike-wave discharges characteristic of generalized epilepsy<sup>14,15,17,18</sup>. Despite the CM being a pivotal node within epileptogenic networks, its relatively small volume and its encasement by white matter tracts, in particular the internal medullary lamina (IML), present significant obstacles for precise electrode targeting to advance neuromodulation therapy<sup>1–3</sup>.

Outcomes from CM stimulation studies have been inconsistent, with some demonstrating substantial seizure reduction and others showing limited or variable efficacy<sup>4–18</sup>. For example, early studies by Velasco et al.<sup>10</sup> reported significant seizure improvement following CM stimulation in patients with generalized epilepsy<sup>10</sup>. However, subsequent studies have yielded mixed results, often attributed to variations in electrode placement accuracy within the CM<sup>4–9,11–18</sup>. Recently, Sisterson et al.<sup>5</sup> disclosed encouraging results with CM stimulation, but surprisingly, almost half of the implantations were outside the CM, highlighting the inconsistencies between targeting intentions and seizure outcomes<sup>5</sup>. These discrepancies underscore the critical need for refined targeting methodologies that consider both anatomical precision and functional assessments of the precise mechanisms underlying CM neuromodulation. Thus, a persistent challenge in the field is the incomplete understanding of these neuromodulatory pathways<sup>8,19,20</sup>.

This study seeks to address these challenges by investigating parameters for CM stimulation through a multimodal approach to elucidate the associated mechanisms of action. Our methodology combines microelectrode recordings (MER) of neuronal activity, intraoperative electrical stimulation, and simultaneous intraoperative electroencephalography (EEG) to deliver real-time feedback on

cortical responses to thalamic stimulation. Additionally, post-implant imaging is employed to determine whether these stimulation sites are located within the CM or adjacent white matter tracts. Using innovative electrophysiological and neuroimaging methods, we demonstrate that stimulating CM target sites with lower neuronal firing activity leads to augmented cortical delta power, suggesting an increase in thalamo-cortical synchronization. We identified these targets in close proximity to the CM, within the intrathalamic white matter tracts that envelop the nucleus. This comprehensive approach seeks to advance the development of evidence-based guidelines for electrophysiological mapping while deepening our understanding of the mechanisms underlying thalamic neuromodulation. By providing critical insights into the precise implantation of thalamic stimulation electrodes in patients with generalized DRE, this study aims to evaluate stimulation locations and elucidate the nuances of CM neuromodulation. Ultimately, these findings, if validated in future clinical studies, are expected to enhance the precision and therapeutic efficacy of neuromodulation strategies for generalized epilepsy.

## Results

To perform MER and macrostimulation of the CM and surrounding areas, we guided microelectrodes with a stereotaxic robot (Fig. 1a). Spectrograms of the sub-scalp EEG far-field potentials during different epochs (pre-stimulation, during stimulation, and post-stimulation), at the different depths for each electrode tract (Figs. 1c and 2b), were calculated based on the power at different EEG frequency bands (alpha, beta, theta, delta, and gamma). Between two macrostimulation contact depths along a single depth electrode trajectory (Fig. 1b and Table 1), we observed at least a 50% difference in the neuronal firing rate between the two macrostimulation contact depths among all subjects (with  $P$ -value < 0.05) (Fig. 2a and Supplementary Fig. 2). The boundaries of the CM were delineated using electrophysiological

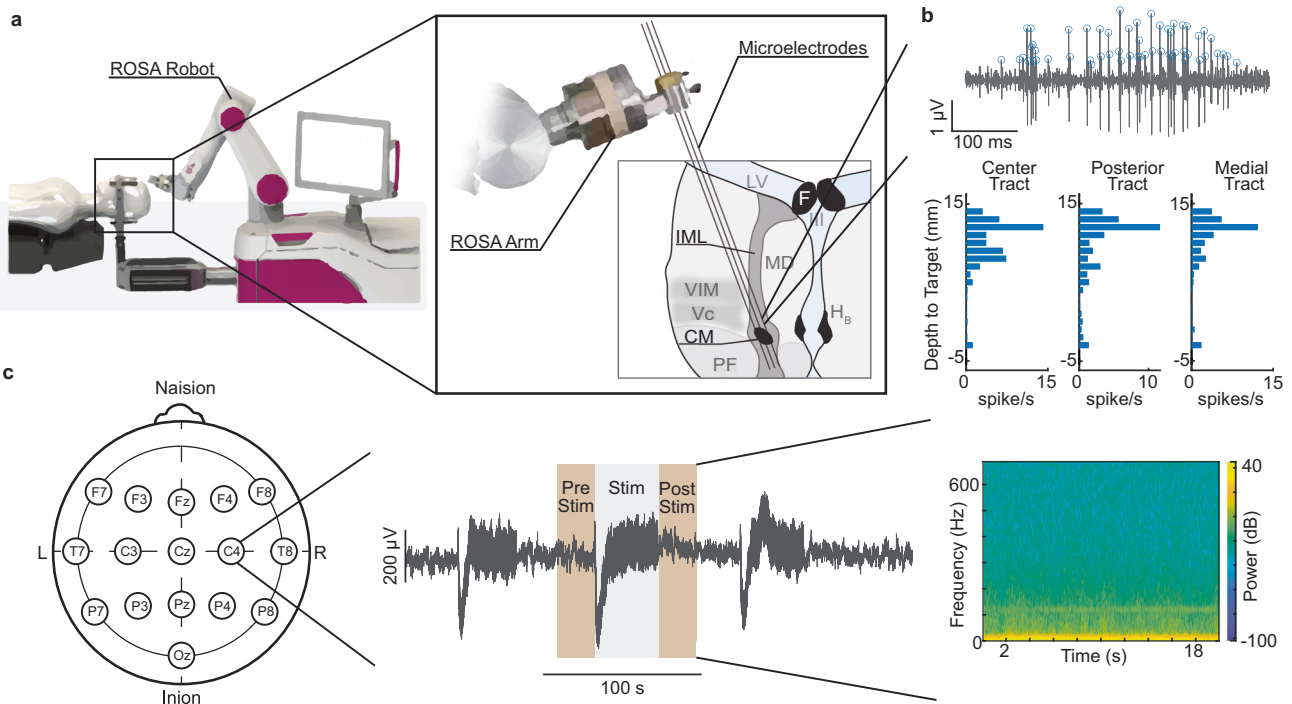


**Fig. 1 | Intraoperative setup and data analysis.** **a** Experimental setup of the ROSA robot advancing three microelectrodes through the CM centromedian nucleus and vicinity, LV lateral ventricle, III third ventricle, H<sub>b</sub> habenula nucleus, MD mediodorsal nucleus, Vc ventral caudal nucleus, VIM ventralis intermedia nucleus, PF parafascicular nucleus, IML internal medullary lamina. **b** *Top*: Example processed trace of the multi-unit data recorded from the microelectrode with the

subsequent peak detection. *Bottom*: An example of the firing rates across all the implant depths is shown **c** *Left*: Map of sub-scalp 10–20 system electroencephalogram (EEG) electrode locations. *Center*: Example sub-scalp EEG trace during stimulation trials. *Right*: Example sub-scalp EEG signal spectrogram during the stimulation phase. Source data for (b, c) are provided as a Source Data file.

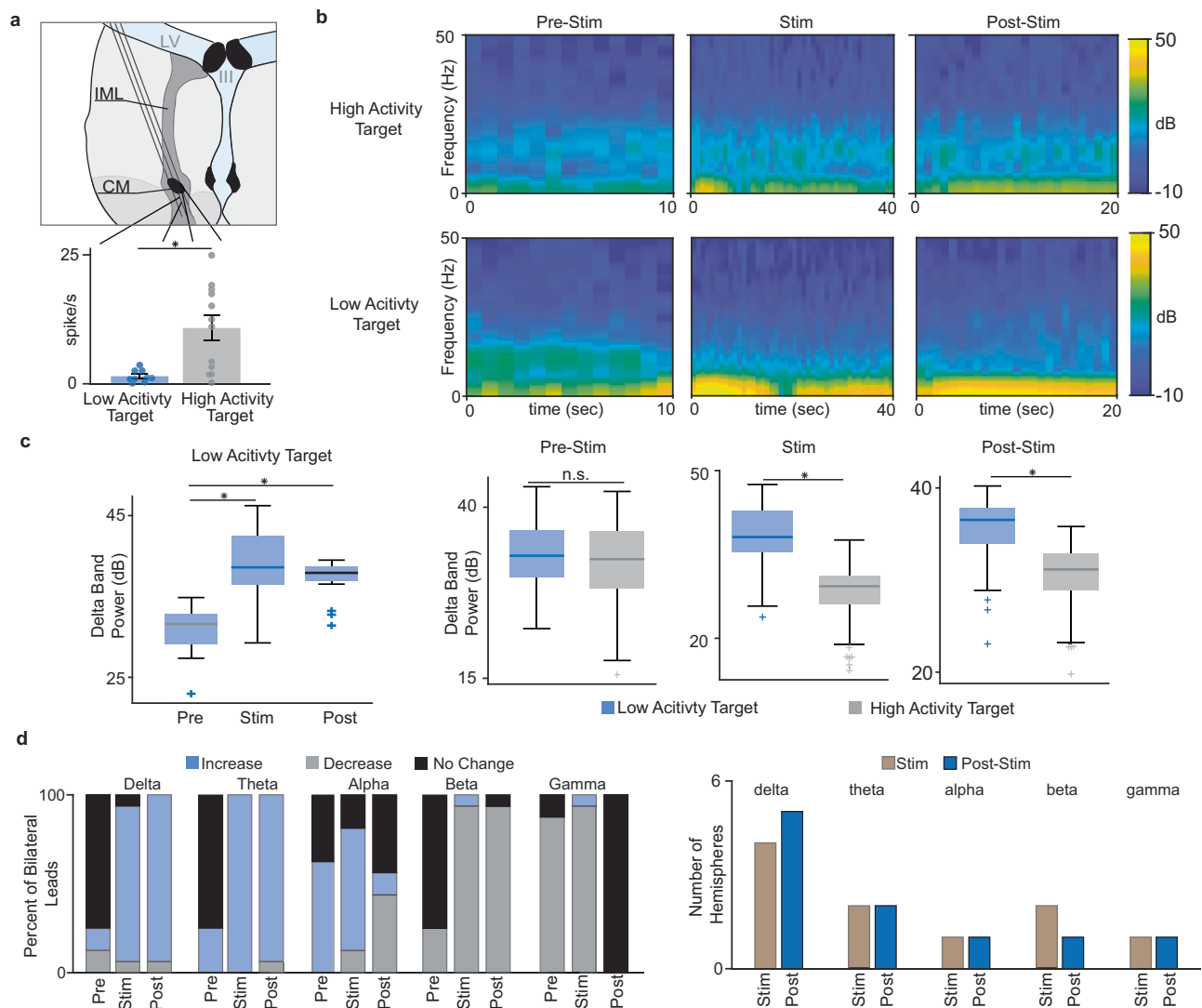


**Fig. 2 | Neuronal firing activity and LFP power in sub-scalp EEG.** **a Top:** Schematic representation of microelectrode recording locations taken near and within the CM centromedian nucleus, LV lateral ventricle, III third ventricle, IML internal medullary lamina. **Bottom:** Multi-unit spiking activity recorded at a low-activity target ( $-1$  mm,  $n = 9$  sites) and a high-activity target ( $+2$  mm,  $n = 12$  sites) along a single microelectrode trajectory of RNS03, RT right tract. Note the difference from recordings inside (higher firing activity) versus outside (lower firing activity) the CM. **b** Example spectrograms during the pre-stimulation (Pre), stimulation (Stim), and post-stimulation (Post) phases at the low and high activity targets. **c Left:** Changes in absolute sub-scalp EEG delta power during the pre-stimulation ( $n = 13$  windows), stimulation ( $n = 50$  windows), and post-stimulation ( $n = 25$  windows) phases during low-activity target stimulation. **Right:** Absolute delta power values when stimulating low and high activity targets along a single electrode trajectory during the pre-stimulation ( $n = 13$  windows,  $n = 13$  windows respectively), stimulation ( $n = 50$  windows,  $n = 50$  windows respectively), and post-stimulation phases

( $n = 25$  windows,  $n = 25$  windows respectively). Here, the stimulation of regions with lower levels of neuronal activity exhibited the highest changes in scalp EEG signals, mainly in the delta band. **d Left:** Percentage of bilateral sub-scalp EEG leads ( $n = 16$ ) that show significant increases, decreases, or no change in power when stimulating low- versus high-activity targets (RNS03 RT) across the delta, theta, alpha, beta, and gamma frequency bands. **Right:** Number of hemispheres displaying potentiation in at least 85% of sub-scalp EEG leads during stimulation and post-stimulation phase of low- versus high-activity targets across each frequency band. For all bar plots, each bar represents the mean, and each error bar represents standard error over trials. For all boxplots, whiskers represent the full data range excluding outliers, and the central, top, and bottom lines denote the median, 25th, and 75th percentiles, respectively. Statistical significance was determined using two-tailed bootstrapping with Bonferroni correction, with significance set at  $p < 0.05$  (\*). Source data for (a–d) are provided as a Source Data file.

criteria. Regions within the nucleus were characterized by higher firing rates (corresponding to high-activity targets), while lower firing rates indicated areas outside or adjacent to the nucleus (corresponding to low-activity targets) (Supplementary Fig. 1). Furthermore, while simultaneously recording sub-scalp EEG during stimulation, microelectrode depths at lower to no neuronal firing activity levels (outside the CM) resulted in a significant increase in the delta power band in sub-scalp EEG compared to depths associated with higher neuronal firing activity levels (within the CM), during both the stimulation and post-stimulation periods (Fig. 2b, c and Supplementary Fig. 3a). Then,

we calculated the proportion of all sub-scalp EEG leads that showed potentiation of various frequency bands when stimulating at the lower neuronal firing activity level. We observed that, when stimulating at the location of lower neuronal firing activity, the delta power band showed the most consistent increase in spectral power across all sub-scalp EEG across the 6 hemispheres we implanted (Fig. 2d and Supplementary Fig. 3b). Yet, no consistent correlations between the two different stimulation depths at any other frequency bands were observed. Five out of six hemispheres showed a significant increase in power in the delta band in greater than 85% of all sub-scalp EEG while no more than

**Table 1 | Demographic data and post-implantation outcomes**

Pt. No.	Age (y)	Sex	Epilepsy duration (y)	Months implanted/ stimulated	Implanted depth along chosen trajectory	Epilepsy diagnosis	Seizure type		Seizure frequency	
							Before RNS	After RNS	Before RNS	After RNS
RNS01	45	F	20	12/7	-1 mm -1 mm	JAE	Absence GTC	-50/day -1-2/week	50-75% reduction None in last 7 mo	
RNS02	26	F	11	11/5	-3.5 mm -3.5 mm	IGE	Absence Myoclonus GTC	-1-10/day -1-10/day -2-3/mo	50-75% reduction 50-75% reduction None in last 2 mo	
RNS03	21	F	8	10/8	-1 mm -1 mm	JAE	Absence	-40/day	50% reduction	

CM centromedian nucleus of the thalamus, GTC general tonic-clonic seizure, JME juvenile myoclonic epilepsy, JGE idiopathic generalized epilepsy, JAE juvenile absence epilepsy, y year, mo months.

2 hemispheres showed such a large proportion of potentiation in the other frequency bands. (Fig. 2d).

Next, we sought to determine the precise location of the stimulation locations with elevated delta power in relation to the intended anatomical target, the CM. Anatomically, it is likely that these low-activity areas outside the CM correspond to the white matter fibers of the IML (Fig. 3a). In all three patients, the implanted RNS electrodes were confirmed to traverse some extent of the CM with the targeted contacts based on the microelectrode stimulation with low neuronal firing activity (most distal contact for RNS01 and RNS03 and 2nd most distal contact for RNS02) identified to be located in proximity, but outside of CM (Fig. 3b).

### Clinical outcomes

No complications related to RNS electrode placement or macrostimulation of the electrode contacts were reported. Each patient's ictal pattern captured in the responsive neurostimulator is illustrated in Supplementary Fig. 4. As illustrated in Table 1, the overall improvement noted in all 3 patients was that no GTC were reported for the last few months of RNS therapy with greater than a 50% average decrease in the number of reported absence and myoclonic seizures.

### Discussion

Our study marks an important advancement in the field of neuromodulation for generalized epilepsy by establishing a correlation between multimodal electrophysiological data, such as neuronal discharge characteristics from MER and stimulation-dependent frequency band power changes in sub-scalp EEG. By using MER to precisely identify stimulation targets with the lowest levels of neuronal activity, we observed that these sites, when stimulated, led to an increase in delta band power. These low-activity target sites, reconstructed to be immediately adjacent to the CM and likely within the IML, provide mechanistic insights into the effects of CM neuromodulation and may offer a deeper understanding of the underlying mechanisms of action of CM neuromodulation. This integrated approach combining MER with sub-scalp EEG monitoring provides a foundation for personalized and electrophysiologically guided implantation of thalamic stimulation electrodes during intraoperative procedures. Such advances are essential for improving the precision and efficacy of neuromodulation therapies in patients with drug-resistant generalized epilepsy.

The results demonstrate that even small changes in depth, only millimeters apart, along a single trajectory can show significant differences in recorded neuronal activity and in stimulation effects on delta band power changes in the sub-scalp EEG. Velasco et al.<sup>11</sup> reported that DBS of the CM could evoke recruiting responses. These responses were characterized by long-latency (around 35 ms) monophasic surface-negative waxing and waning EEG potentials, recorded from the sub-scalp during the stimulation phase. The stimulation was delivered at a frequency of 6–8 Hz, with a pulse duration of 0.45 ms and intensities ranging from 0.8 to 1.2 mA. The author reported that this suggests a specific brain activity pattern in response to stimulation, which could be relevant in the context of neuromodulation strategies for epilepsy and other neurological disorders. In our patient cohort, we did not observe the recruitment patterns previously described, which pertain to the distinct temporal sequence and mode of neuronal activation in response to specific external stimuli. These previously observed oscillatory patterns differ from the activity recorded in our current experiments, as did our stimulation parameters. Our protocol employed higher stimulation frequencies (147 Hz vs. 6–8 Hz), greater stimulus intensities (3.0 mA vs. 0.8–1.2 mA), and shorter pulse durations (0.16 ms vs. 0.45 ms). Under these conditions, we observed localized increases in delta band activity (Fig. 2, Supplementary Figs. 2, 3, and 5a) that emerged during stimulation and persisted post-stimulation. The sustained elevation in cortical delta activity post-stimulus provides further evidence that our findings

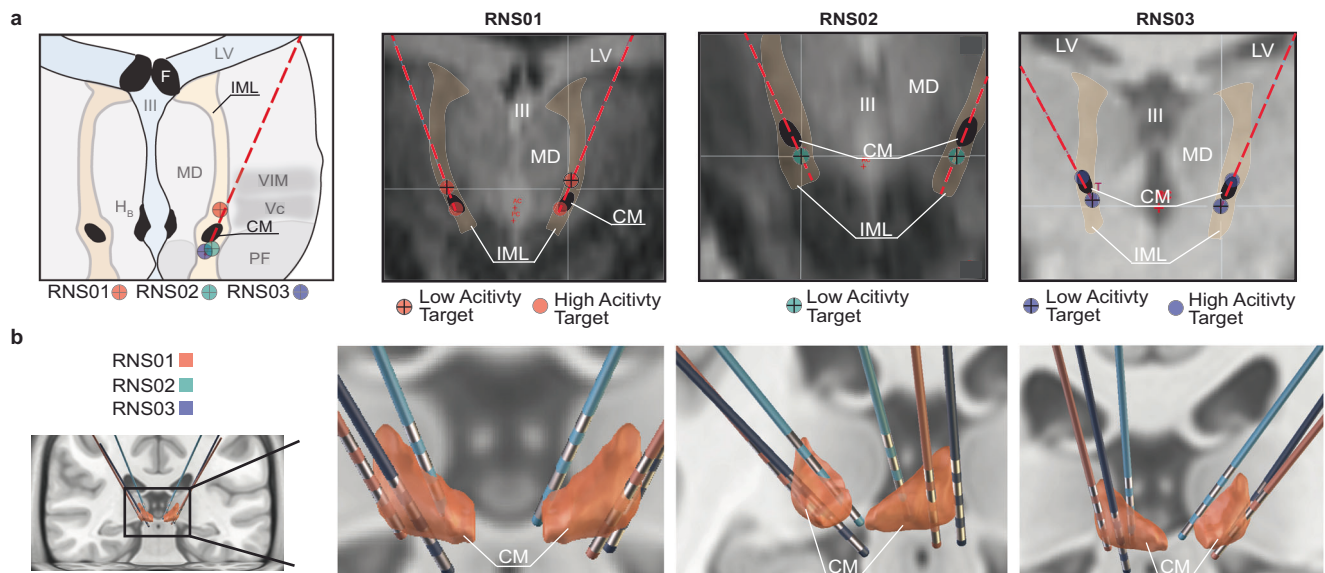


**Fig. 3 | Localization of Stimulation locations across Hemispheres.** **a Left:** Localization of stimulation locations that caused the greatest increase in delta band power. LV lateral ventricle, III third ventricle, H<sub>B</sub> habenula nucleus, MD mediodorsal nucleus, CM centromedian nucleus, Vc ventral caudal nucleus, VIM ventralis

intermediate nucleus, PF parafascicular nucleus, IML internal medullary lamina. **Right:** FGATIR-MRI and T2 of the location of each stimulation location.

**b Reconstruction of final electrode implantation for each subject using group analyses with lead-DBS<sup>39</sup> and Human Motor Thalamus atlas<sup>40</sup>.**

diverge from previously reported recruitment patterns, which were confined to the stimulation period. Short-term follow-up studies of these patients revealed a significant reduction in seizure incidence, indicating a positive clinical outcome associated with the stimulation protocol. However, future clinical trials are warranted to assess the differences in outcomes between patients receiving stimulation involving the IML versus those receiving only CM stimulation.

We then demonstrate that putative white matter stimulation, corresponding to the IML, rather than the targeted CM stimulation, is associated with the greatest level of cortical electrophysiological responses in the delta band frequency range. Our method establishes a framework of real-time feedback using intraoperative neurophysiological data, enabling the clinical team to make immediate adjustments to enhance the accuracy of thalamic electrode placement. This approach is crucial for optimizing RNS therapy<sup>11</sup>. Although demonstrated for Zona Incerta DBS therapy in PD<sup>21</sup>, the targeting of white matter tracts typically diverges from conventional and well-established methods for DBS implantation in movement disorders and is an alternative proposal for thalamic neuromodulation for seizure control. For example, the optimal placement of DBS electrodes in patients with Parkinson's disease is targeted to regions of the STN with the highest cell density and largest STN span by unitary recordings<sup>22</sup>. Here, the opposite may be true for CM stimulation for generalized epilepsy, since we find that stimulation locations with low neuronal activity, likely within the IML white matter bundle surrounding the CM, could provide more beneficial clinical effects.

Our data suggest that stimulation targets that produce the largest elevation of cortical delta power are immediately adjacent to the CM. Our preliminary analysis indicates that this white matter likely corresponds to the IML. The IML is a crucial yet underexplored thalamic structure in the context of seizure reduction. It is a thin layer of myelinated nerve fibers traversing the central region of the thalamus, dividing it into medial and lateral components<sup>23–26</sup>. The IML surrounds the CM and facilitates bidirectional projections to and from various cortical areas. It plays a pivotal role in thalamic organization and connectivity, serving as an essential relay station for sensory and motor signals<sup>27–30</sup>. Additionally, as part of the reticular formation, the IML is involved in regulating cortical excitability, with widespread

influence over cortical activity, particularly during sleep and wakefulness<sup>3</sup>. Here, the bilateral effects of electrical stimulation in the vicinity of the CM are intriguing and likely reflecting the widespread influence of delta power changes, which may be attributed to the extensive bilateral projections of the IML. In a recent publication, our group highlighted similar findings in other thalamic regions, demonstrating the modulation of bi-hemispheric epileptic activity through unilateral thalamic stimulation<sup>31,32</sup>. This expansive network, which includes projections to critical structures such as the cerebral peduncles, provides a plausible explanation for the observed effects across both hemispheres and the multiple sub-scalp electrodes recorded<sup>3</sup>. The IML's involvement in epileptic mechanisms, particularly those affecting consciousness and alertness, highlights its significance since disruptions in consciousness and alertness are critical factors contributing to morbidity and a decline in quality of life in patients with generalized epilepsy. Importantly, further investigation is warranted to replicate our results of a widely distributed increase in delta power following stimulation in the IML.

The sole consistent EEG frequency modulation that increased in power with CM stimulation was observed in the delta-band activity. Studies have demonstrated that cortical delta activity is thalamus-driven, occurring when thalamocortical neurons transition to a burst mode of firing, effectively isolating cortical neurons from sensory input<sup>33,34</sup>. Thalamic bursting, induced by rebound excitation when thalamocortical neurons are rapidly released from inhibition, occurs at delta frequencies. This process may toggle cortical pyramidal cells between up and down states at the same frequency while obstructing ascending sensory input<sup>35,36</sup>. Noteworthy is the correlation between the deactivation of the thalamus, measured by regional cerebral blood flow, and the emergence of delta oscillations<sup>37</sup>. Taking this into consideration, we assert that the stimulation-induced increase in delta power acts as a biomarker in locating an optimal target within the vicinity of the CM for thalamic neuromodulation and potential anti-epileptic effects. This proposal suggests that the ability for fine adjustments of the final implant location can be based on electrophysiological data, such as modulated delta power in the EEG. Future studies are required to assess if this biomarker-assisted targeting of IML for neuromodulation therapies can reliably lead to long-term

seizure reduction as we have shown some short-term results in this limited cohort of DRE patients.

Our study has limitations. While it is based on intraoperative data recorded under anesthesia, the robustness and consistency of our results are noteworthy. The effectiveness of IML/CM stimulation guided by the described method in long-term seizure control and a larger cohort of patients warrants further investigation. Additionally, although our results were acquired from a relatively small cohort of patients, the use of several recording and stimulating sites (36 in total) demonstrates high consistency and robustness, enhancing the reliability of our findings.

In conclusion, the results of different multi-unit recordings and electrical stimulation locations within the CM and adjacent areas demonstrated that the targets with lower neuronal density, potentially indicating axon-predominant regions, were associated with widespread cortical delta band frequency changes. We determined that the thalamic structure corresponding to the lower neuronal density regions to most likely be the IML. These findings contribute to a deeper understanding of the underlying mechanisms of action of CM-targeted neuromodulation therapy. This approach, which integrates MER mapping with sub-scalp EEG monitoring, paves the way for personalized and electrophysiologically guided intraoperative implantation of thalamic stimulation electrodes in treating generalized epilepsy.

## Methods

### Human participants

This study was performed under a University of Pittsburgh Institutional Review Board approved protocol (STUDY21060089). From 2022 to 2023, we consecutively enrolled  $n = 3$  patients (3 females) of age  $30.7 \pm 12.6$  (mean  $\pm$  s.d.) who underwent bilateral responsive nerve stimulator (RNS) implantations of the CM for DRE (Table 1). The participants were informed of the procedure, and they signed an informed consent, which included the consent for the use of all collected data. Bilateral hemispheric studies were performed for each subject. For each studied hemisphere, three different tracts of recording and stimulation, at 2 different depth levels, were recorded and analyzed with a total of 36 studied sites. All subjects had failed at least two appropriate doses of chosen antiepileptic medications and were considered non-resection candidates due to the diagnosis of generalized DRE. After multidisciplinary case management discussions, all patients were decided to be implanted with RNS systems (Neuropace, Mountain View, CA, USA) with robotic stereotaxic guidance (ROSA, Zimmer-Biomet, Warsaw, IN, USA) and bone fiducial registration (Fig. 1a). Pre-operative MRI and CT were acquired to determine the pre-operative stereotactic plan and target location within the CM in relation to the AC-PC (anterior commissure-posterior commissure) line. Stereotactic coordinates for the indirect target were originally defined as 6 mm lateral to the AC-PC line, 1 mm dorsal to the AC-PC line, and 1 mm rostral to the vertical line through the PC. The final target coordinates were further refined by the direct visualization of the CM using Fast Gray Matter Acquisition T1 Inversion Recovery (FGATIR) or T2-weighted MRI images (1 mm isotropic, TR/TE = 2300/2.9 ms, 3T Siemens-Prisma Fit)<sup>38</sup>.

Before the operation started, a Leksell stereotactic frame was applied to each patient, and 10–20 sub-scalp EEG electrodes were placed by the neurophysiologists (TA, DJC). Sub-scalp EEG recordings (13 mm Needle Electrodes, Rhythmlink, Columbia, SC, USA) were continuously recorded throughout the operation until after placement of the depth electrodes.

### Intra-operative electrophysiology

For all three patients, intravenous propofol and sevoflurane were used to induce sedation. After induction, IV remifentanyl and dexmedetomidine were utilized for maintenance. No changes in anesthesia were made throughout the MER and stimulation phases of the surgery.

Before the final implantation of the depth electrodes, MER mapping of the CM and vicinity areas was performed and interpreted by the senior neurophysiologist (DJC). Three sterile Sonus NeuroProbe microelectrodes (Alpha Omega, Nof HazGilil, Israel) were used to map the CM and adjacent areas (Fig. 1a). The three microelectrodes were positioned within a “Ben-Gun” microelectrode holder’s center, posterior, and medial trajectories (2 mm between each trajectory). They were advanced with a NeuroFortis head stage (Alpha Omega, Nof HazGilil, Israel). MER began 13–15 mm above the pre-determined CM target depth and ended, on average, at 4 mm below the target (Supplementary Fig. 1). Single and multi-unit action potentials were recorded as the three microelectrodes were simultaneously advanced along the three pre-defined trajectories (Fig. 1b). During this process, two depths of higher (high activity target) and lower (low activity target) firing activity were identified intra-operatively at which monopolar stimulation through the macro-contact of each of the three electrodes, was tested sequentially at a current of 3.0 mA, frequency of 147 Hz, and a pulse width of 160 ms for 40 s, closely mimicking the default stimulation parameters of bipolar RNS. Stimulation was performed in each of the three tracts at two different depths and was repeated twice. Stimulation testing was delayed for 2 min between stimulation sessions to permit the EEG signal to recover to baseline values. The site that resulted in the maximum stimulation-induced delta activity in the sub-scalp EEG was determined and used for the final RNS electrode placement (Table 1).

### Analysis of sub-scalp EEG and multi-unit activity

Sixteen sub-scalp EEGs were placed using a 10–20 EEG placement system and recorded in a referential montage to the mastoid bone (Fig. 1c). The sampling rate of the sub-scalp EEG was 1275 Hz. We conducted a frequency power analysis of sub-scalp EEG data across three distinct phases: a 10-s pre-stimulation phase before any stimulation was applied, a 40-s stimulation phase, and a 20-s post-stimulation phase (Fig. 1c). This analysis was performed at two different depths and repeated for each trial. To calculate the power in each frequency band, we applied a short-time Fourier transform to the EEG signals, focusing on the following bands: delta (0.5–4 Hz), theta (4–8 Hz), alpha (8–13 Hz), beta (13–30 Hz), and gamma (30–100 Hz). Power values were expressed in decibels (dB) for each frequency band. Then, the number of interictal epileptiform discharges were counted and confirmed by the neurologist (TA) during the 20 s post-stimulation phase.

For multi-unit detection, we performed bandpass filtering of gross MER data from 300 to 3000 Hz and calculated the derivative of the filtered signal. To detect neuronal spiking units, we found peaks above a threshold of three to six standard deviations of the entire signal. We divided the number of spikes by the length of the signal in seconds to compute the firing rate and estimated the level of neuronal firing activity recorded at each depth.

### Statistical procedure

All statistical comparisons of means were performed using the bootstrap method, a non-parametric approach that makes no distributional assumptions on the observed data. For each comparison, we construct bootstrap samples by drawing a sample with replacement from observed measurements, while preserving the number of measurements in each condition. We construct 10,000 bootstrap samples and, for each, calculate the difference in means of the resampled data. We employed two-tailed bootstrapping with alphas of 0.05 (95% confidence interval). The null hypothesis of no difference in the mean was rejected if 0 was not included in the confidence interval of the corresponding alpha value. If more than one comparison was being performed at once, we used a Bonferroni correction by dividing the alpha value by the number of pairwise comparisons being performed.

### Data analysis software

Data analysis of cortical and thalamic neural data was performed using custom analysis code written in Matlab R2021a/b. Data from intra-operative electrophysiology were extracted manually and converted to Matlab files from proprietary data files using the Neuro Omega File Converter (v.5.1.10). Electrode reconstructions was performed using Lead-DBS (v.2.0) and Compumedics Neuroscan's Curry software (v.9). All figures were rendered in Adobe Illustrator CC (v26.0 - v26.3.1).

### Reporting summary

Further information on research design is available in the Nature Portfolio Reporting Summary linked to this article.

### Data availability

The main data supporting the results in this study are available within the paper and its Supplementary Information. Source data are provided with this paper. Due to the sensitive nature of the dataset, which contains graphic information on human patients, raw data are available under restricted access and access can be obtained upon request to the corresponding author (Gonzalez-Martinez; gonzalezjo@upmc.edu). Data access will be provided within a month from the request and for up to 6 months once access has been granted. Source data are provided with this paper.

### Code availability

Software routines utilized for data analysis will be deposited on GitHub under search keyword NCOMMS-24-17835B and the following link: <https://github.com/jho323/NCOMMS-24-17835B>.

### References

- Ilyas, A., Pizarro, D., Romeo, A. K., Riley, K. O. & Pati, S. The centromedian nucleus: anatomy, physiology, and clinical implications. *J. Clin. Neurosci.* **63**, 1–7 (2019).
- Dalic, L. J. et al. Cortex leads the thalamic centromedian nucleus in generalized epileptic discharges in Lennox-Gastaut syndrome. *Epilepsia* <https://doi.org/10.1111/epi.16657> (2020).
- Kumar, V. J., Scheffler, K. & Grodd, W. The structural connectivity mapping of the intralaminar thalamic nuclei. *Sci. Rep.* <https://doi.org/10.1038/s41598-023-38967-0> (2023).
- Gregg, N. M. et al. Thalamic deep brain stimulation modulates cycles of seizure risk in epilepsy. *Sci. Rep.* **11**, 24250 (2021).
- Sisterson, N. D., Kokkinos, V., Urban, A., Li, N. & Richardson, R. M. Responsive neurostimulation of the thalamus improves seizure control in idiopathic generalised epilepsy: initial case series. *J. Neurol. Neurosurg. Psychiatry* <https://doi.org/10.1136/jnnp-2021-327512> (2022).
- Kwan, P. et al. Definition of drug resistant epilepsy: consensus proposal by the ad hoc Task Force of the ILAE commission on therapeutic strategies. *Epilepsia* **51**, 1069–1077 (2010).
- Fisher, R. S. Deep brain stimulation of thalamus for epilepsy. *Neurobiol. Dis.* **179**, 106045 (2023).
- Dalic, L. J. et al. DBS of thalamic centromedian nucleus for Lennox-Gastaut Syndrome (ESTEL Trial). *Ann. Neurol.* <https://doi.org/10.1002/ana.26280> (2022).
- Fields, M. C. et al. A multicenter retrospective study of patients treated in the thalamus with responsive neurostimulation. *Front. Neurol.* **14**, 1202631 (2023).
- Velasco, F., Velasco, M., Ogarrio, C. & Fanghanel, G. Electrical stimulation of the centromedian thalamic nucleus in the treatment of convulsive seizures: a preliminary report. *Epilepsia* <https://doi.org/10.1111/j.1528-1157.1987.tb03668.x> (1987).
- Velasco, F. et al. Predictors in the treatment of difficult-to-control seizures by electrical stimulation of the centromedian thalamic nucleus. *Neurosurgery* <https://doi.org/10.1097/00006123-200008000-00007> (2000).
- Fisher, R. S. et al. Placebo-controlled pilot study of centromedian thalamic stimulation in treatment of intractable seizures. *Epilepsia* <https://doi.org/10.1111/j.1528-1157.1992.tb02192.x> (1992).
- Torres Diaz, C. V. et al. Network substrates of centromedian nucleus deep brain stimulation in generalized pharmacoresistant epilepsy. *Neurotherapeutics* <https://doi.org/10.1007/s13311-021-01057-y> (2021).
- Cui, Z. et al. Long-term efficacy of deep brain stimulation of the subthalamic nucleus in patients with pharmacologically intractable epilepsy: a case series of six patients. *Epileptic Disord.* <https://doi.org/10.1002/epd2.20129> (2023).
- Li, T., Deng, J., Qin, J. & Chu, X.-P. Editorial: neuromodulation for pharmacoresistant epilepsy: from bench to bed. *Front. Neurol.* **15**, 1354897 (2024).
- Dembek, T. A. et al. Directional DBS leads show large deviations from their intended implantation orientation. *Park. Relat. Disord.* <https://doi.org/10.1016/j.parkreldis.2019.08.017> (2019).
- Fisher, R. et al. Electrical stimulation of the anterior nucleus of thalamus for treatment of refractory epilepsy. *Epilepsia* <https://doi.org/10.1111/j.1528-1167.2010.02536.x> (2010).
- Gesche, J., Christensen, J., Hjalgrim, H., Rubboli, G. & Beier, C. P. Epidemiology and outcome of idiopathic generalized epilepsy in adults. *Eur. J. Neurol.* <https://doi.org/10.1111/ene.14142> (2020).
- Yeh, F. C. et al. Population-averaged atlas of the macroscale human structural connectome and its network topology. *Neuroimage* <https://doi.org/10.1016/j.neuroimage.2018.05.027> (2018).
- Yeh, F. C. et al. Automatic removal of false connections in diffusion MRI tractography using topology-informed pruning (TIP). *Neurotherapeutics* <https://doi.org/10.1007/s13311-018-0663-y> (2019).
- Ossowska, K. Zona incerta as a therapeutic target in Parkinson's disease. *J. Neurol.* **267**, 591–606 (2020).
- Lu, C. W., Malaga, K. A., Chou, K. L., Chestek, C. A. & Patil, P. G. High density microelectrode recording predicts span of therapeutic tissue activation volumes in subthalamic deep brain stimulation for Parkinson disease. *Brain Stimul.* <https://doi.org/10.1016/j.brs.2019.11.013> (2020).
- Jones, E. G. *The Thalamus* (Cambridge University, 2007).
- Nowinski, W. L. Anatomical targeting in functional neurosurgery by the simultaneous use of multiple Schaltenbrand-Wahren brain atlas microseries. *Stereotact. Funct. Neurosurg.* **71**, 103–116 (1998).
- Niemann, K., Mennicken, V. R., Jeanmonod, D. & Morel, A. The Morel stereotactic atlas of the human thalamus: atlas-to-MR registration of internally consistent canonical model. *Neuroimage* **12**, 601–616 (2000).
- Schaltenbrand, G. & Wahren, W. *Atlas for Stereotaxy of the Human Brain* (Year Book Medical Publishers, 1977).
- Albe-Fessard, D. & Besson, J. M. Convergent thalamic and cortical projections --- the non-specific system. in *Somatosensory System* (ed. Iggo, A.) 489–560 (Springer Berlin Heidelberg, 1973). [https://doi.org/10.1007/978-3-642-65438-1\\_14](https://doi.org/10.1007/978-3-642-65438-1_14).
- Guilbaud, G., Berkley, K. J., Benoist, J. M. & Gautron, M. Responses of neurons in thalamic ventrobasal complex of rats to graded distension of uterus and vagina and to uterine suprafusion with bradykinin and prostaglandin F<sub>2</sub> alpha. *Brain Res.* **614**, 285–290 (1993).
- Matsumoto, N., Minamimoto, T., Graybiel, A. M. & Kimura, M. Neurons in the thalamic CM-Pf complex supply striatal neurons with information about behaviorally significant sensory events. *J. Neurophysiol.* **85**, 960–976 (2001).
- Peschanski, M., Guilbaud, G. & Gautron, M. Posterior intralaminar region in rat: neuronal responses to noxious and nonnoxious cutaneous stimuli. *Exp. Neurol.* **72**, 226–238 (1981).

31. Ikegaya, N. et al. Thalamic stereoelectroencephalography for neuromodulation target selection: Proof of concept and review of literature of pulvinar direct electrical stimulation. *Epilepsia* **65**, e79–e86 (2024).
  32. Zhang, R. et al. Temporal-spatial characteristics of phase-amplitude coupling in electrocorticogram for human temporal lobe epilepsy. *Clin. Neurophysiol.* **128**, 1707–1718 (2017).
  33. Walter, W. G. The electro-encephalogram in cases of cerebral tumour. *J. R. Soc. Med.* **30**, 579–598 (1937).
  34. Steriade, M. Corticothalamic resonance, states of vigilance and mentation. *Neuroscience* [https://doi.org/10.1016/S0306-4522\(00\)00353-5](https://doi.org/10.1016/S0306-4522(00)00353-5) (2000).
  35. Buzsáki, G. *Rhythms of the Brain* (Oxford University Press, 2009). <https://doi.org/10.1093/acprof:oso/9780195301069.001.0001>.
  36. Frank, N. P. General anaesthesia: from molecular targets to neuronal pathways of sleep and arousal. *Nat. Rev. Neurosci.* <https://doi.org/10.1038/nrn2372> (2008).
  37. Hofle, N. et al. Regional cerebral blood flow changes as a function of delta and spindle activity during slow wave sleep in humans. *J. Neurosci.* <https://doi.org/10.1523/jneurosci.17-12-04800.1997> (1997).
  38. Sudhyadhom, A., Haq, I. U., Foote, K. D., Okun, M. S. & Bova, F. J. A high resolution and high contrast MRI for differentiation of subcortical structures for DBS targeting: the Fast Gray Matter Acquisition T1 Inversion Recovery (FGATIR). *Neuroimage* <https://doi.org/10.1016/j.neuroimage.2009.04.018> (2009).
  39. Treu, S. et al. Deep brain stimulation: imaging on a group level. *Neuroimage* **219**, 117018 (2020).
  40. Ilinsky, I. et al. Human motor thalamus reconstructed in 3D from continuous sagittal sections with identified subcortical afferent territories. *eNeuro* **5**, ENEURO.0060-18.2018 (2018).
- surgery. A.M. assisted with all surgeries. D.C. performed the subcortical mapping of CM for the human DBS implantations. D.C. and T.A. collected the MER and sub-scalp EEG data. J.H. analyzed the neural data. T.A. reconstructed deep brain electrodes. D.C., J.G.M., A.M., A.D., and L.T. helped with data interpretation. J.H., T.A., D.C., and J.G.M. wrote the paper and all authors contributed to its editing.

## Competing interests

The authors declare no competing interests.

## Additional information

**Supplementary information** The online version contains supplementary material available at <https://doi.org/10.1038/s41467-025-60183-9>.

**Correspondence** and requests for materials should be addressed to Jorge A. González-Martínez.

**Peer review information** *Nature Communications* thanks Stephan Chabardes, Andreas Horn, and the other anonymous reviewer(s) for their contribution to the peer review of this work. A peer review file is available.

**Reprints and permissions information** is available at <http://www.nature.com/reprints>

**Publisher's note** Springer Nature remains neutral with regard to jurisdictional claims in published maps and institutional affiliations.

**Open Access** This article is licensed under a Creative Commons Attribution-NonCommercial-NoDerivatives 4.0 International License, which permits any non-commercial use, sharing, distribution and reproduction in any medium or format, as long as you give appropriate credit to the original author(s) and the source, provide a link to the Creative Commons licence, and indicate if you modified the licensed material. You do not have permission under this licence to share adapted material derived from this article or parts of it. The images or other third party material in this article are included in the article's Creative Commons licence, unless indicated otherwise in a credit line to the material. If material is not included in the article's Creative Commons licence and your intended use is not permitted by statutory regulation or exceeds the permitted use, you will need to obtain permission directly from the copyright holder. To view a copy of this licence, visit <http://creativecommons.org/licenses/by-nc-nd/4.0/>.

© The Author(s) 2025

## Acknowledgements

We thank Isabella Bushko for the design of figure elements, and Eliza Reddy and Michaela Lionetti for acquiring the patients' MRI and CT scans. We also wish to thank all UPMC operating room staff, UPMC physicians, patients, and their families for their support of this project.

The study was executed through the support of internal funding from the Department of Neurological Surgery at the University of Pittsburgh JGM. Additionally, J.G.M. discloses support for the research described in this study from the Hamot Health Foundation. Finally, this work was supported by the National Institutes of Health (R01NS122927 to J.G.M.).

## Author contributions

J.G.M. and T.A. conceived the study. J.G.M. secured funding. J.H., T.A., D.C., and J.G.M. designed the experiments. J.G.M. performed the